Symmetry of spatial-dispersion-induced birefringence and its implications for CaF_2 ultraviolet optics

John H. Burnett
National Institute of Standards and Technology
Building 221, Room B228
Gaithersburg, Maryland 20899-8421
E-mail: john.burnett@nist.gov

Zachary H. Levine
National Institute of Standards and Technology
Building 245, Room B102
Gaithersburg, Maryland 20899-8410

Eric L. Shirley
National Institute of Standards and Technology
Building 221, Room B208
Gaithersburg, Maryland 20899-8441

John H. Bruning
Corning Tropel Corporation
60 O'Connor Road
Fairport, New York 14450

Abstract. The discovery of a significant spatial-dispersion-induced birefringence (intrinsic birefringence) in CaF_2 at ultraviolet wavelengths has had a major impact on the design of 157 nm lithography systems, requiring complete redesign of the optics to take account of the imaging aberrations resulting from the birefringence and the accompanying index anisotropy. This intrinsic birefringence phenomena results from a symmetry-breaking effect of the finite wave vector of the photon on the symmetry of the light-matter interaction in fluorite-structure cubic crystals. As a follow-up to our original concise report of measurements and theory of the effect in CaF_2 and BaF_2, we present here a more detailed analysis of the theory, focusing on the symmetry and its consequences. We also provide the full directional dependence of the effect in useful closed forms. We analyze the implications for precision optical design with CaF_2 optical elements, and discuss qualitatively the approaches being considered to compensate for it. [DOI: 10.1117/1.1503350]

Subject terms: birefringence; spatial dispersion; symmetry; calcium fluoride; CaF_2; barium fluoride; BaF_2.

Paper 102007 JM3 received Apr. 12, 2002; revised manuscript received July 3, 2002; accepted for publication July 8, 2002.

1 Introduction

When the semiconductor industry began to consider developing optical lithography based on illumination wavelengths below 248 nm, the system designers were forced to incorporate crystalline material in the optics, due to the optical limitations of available amorphous materials. For 193 nm lithography a second material, such as CaF_2, would be needed for combination with fused silica for correction of chromatic aberrations. At 157 nm no practical amorphous material is transmissive enough, and it was clear that the refractive optics would have to be made entirely of crystalline materials, with CaF_2 being the principal candidate. Though crystalline materials in general have anisotropic optical properties and natural birefringence, it was widely thought that for crystals with cubic crystal symmetry such as CaF_2, birefringence and index anisotropy were symmetry forbidden in perfect crystals at sub-bandgap photon energies. Only *extrinsic* symmetry-breaking effects such as strain could allow these. Experience with CaF_2 at visible wavelengths seemed to confirm this. Thus, it came as a surprise to the industry when measurements and accompanying analysis showed that there was in fact an *intrinsic* birefringence and index anisotropy in CaF_2, and that the magnitudes were far larger than tolerable.[1–3] Fortunately, the symmetry-breaking effect responsible for this still preserves rather high symmetry. This has enabled correction schemes which, though complicating the designs, have been shown to work in simulations.

The analysis of the effect in the original work was presented in a very concise form,[3] leaving out most of the details, resulting in some confusion and controversy. The purpose of this paper is to expand on the original analysis, giving a thorough, rigorous treatment of the details, derivations of key results, and a more complete analysis of the implications for optics. Section 2 of this paper briefly discusses the history of the investigation of the effect. Section 3 presents the theory of spatial-dispersion-induced birefringence (intrinsic birefringence) in cubic crystals. The implications for optics are briefly examined in Sec. 4, including a qualitative discussion of the correction approaches proposed. Concluding remarks are given in Sec. 5.

2 History

The origin of the intrinsic birefringence and the accompanying index anisotropy in cubic crystals is the finite wave vector of light $\mathbf{q}$, which breaks the lowest-order isotropic symmetry of the light-matter interaction in cubic crystals. Lorentz, best known for the Lorentz transformation of the theory of relativity, first considered this small symmetry-breaking effect in ''regular crystals'' in 1878,[4] before the formulation of the macroscopic Maxwell equations and over 30 yrs. before the confirmation of the existence of

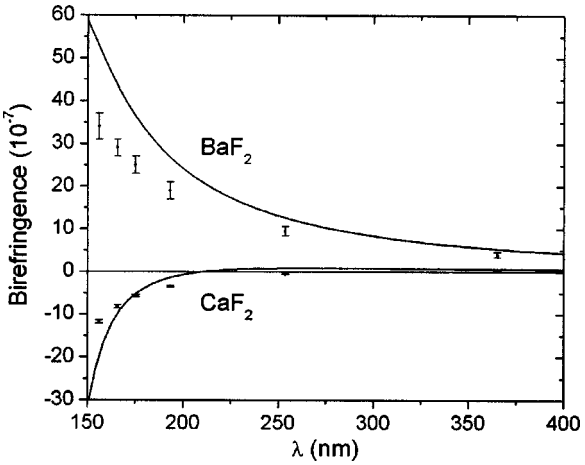

Fig. 1 Measurements (symbols) and calculations (curves) of the intrinsic birefringence ($n_{\langle\bar{1}10\rangle} - n_{\langle 001\rangle}$) in CaF_2 and BaF_2 as functions of wavelength (see Ref. 3). Both measurement and calculation show short wavelength divergent behavior for both materials with opposite signs, and a sign change for CaF_2.

crystal lattices by Bragg and Laue. Lorentz worked out the basic theory of the effect by 1921 and attempted to measure it in NaCl.[5]

This spatial-dispersion-induced (**q**-induced) birefringence in cubic crystals was first convincingly demonstrated by Pastrnak and Vedam in Si in the infrared in 1971,[6] and then by Yu and Cardona in GaAs.[7] Since these and other measured values (see references cited in Ref. 3) were very small and generally in nonoptical materials, these results were viewed as curiosities. Measurements were not made on materials important for optics, and the implications of the effect for precision ultraviolet (UV) optics were not anticipated. In any case, the lithography optics community was apparently unaware of this effect when it began developing systems incorporating CaF_2 optics for 193 and 157 nm lithography in the mid-1990s.

In May of 2001, Burnett, Levine, and Shirley[1] first reported measurements and calculations of intrinsic birefringence in CaF_2, and later BaF_2.[2,3] They presented an analysis of the propagation-direction dependence of the intrinsic birefringence and the accompanying index anisotropy, along with their implications for precision optics in the UV. They also proposed an approach for correcting the effect based on crystal axis clocking[1–3] and an approach to eliminate the effect altogether at a given wavelength based on mixed solid solutions of CaF_2 and BaF_2[2,3] or of CaF_2 and SrF_2.[8] The measurements and first-principles calculations for CaF_2 and BaF_2 are presented in Fig. 1 and in Table 1.[3] Details of the measurement procedures have been presented previously and will not be discussed here.[3] The results have since been confirmed,[9] and detailed analyses of correction strategies have been presented.[10–12]

3 Theory

The optical properties of crystalline materials are characterized by the complex dielectric tensor ϵ_{ij} which describes the effect of the polarizability of the material on the electric field components (E_i) to give the electric displacement field components (D_i). In terms of the inverse dielectric tensor ϵ_{ij}^{-1}, the components of the two fields are related by

$$E_i = \sum_j \epsilon_{ij}^{-1} D_j , \tag{1}$$

where the sum, as always in this paper unless otherwise stated, is over the three Cartesian coordinate directions x_1, x_2, and x_3. For plane waves of frequency ω and wave vector **q**, propagating in the crystal in the direction $\mathbf{q}/|\mathbf{q}| = \hat{\mathbf{q}}$, E_i and D_i have their spatial and time behavior governed by $e^{i(\mathbf{q}\cdot\mathbf{r}-\omega t)}$. In general, ϵ_{ij}^{-1} has a frequency and wave-vector dependence $\epsilon_{ij}^{-1} = \epsilon_{ij}^{-1}(\omega,\mathbf{q})$. At frequencies in the transparent region, $\epsilon_{ij}^{-1}(\omega,\mathbf{q})$ is real, and it can also be shown by energy considerations that $\epsilon_{ij}^{-1}(\omega,\mathbf{q})$ is symmetric under the interchange $i \leftrightarrow j$.[13] For the magnitude of **q** much smaller than the size of the Brillouin zone, or equivalently, the wavelength λ much larger than the size of the unit cell, the spatial dispersion effects of **q** can be neglected and $\epsilon_{ij}^{-1}(\omega,\mathbf{q})$ can be taken to be independent of **q** [i.e., $\epsilon_{ij}^{-1}(\omega,\mathbf{q}) \approx \epsilon_{ij}^{-1}(\omega,0)$].

The tensor $\epsilon_{ij}^{-1}(\omega,\mathbf{q})$ must obey the symmetry of the light-matter interaction. Assuming $\mathbf{q}=0$, this means that $\epsilon_{ij}^{-1}(\omega,0)$ must obey the symmetry of the crystal. CaF_2 has the cubic fluorite crystal structure (space group: $Fm3m$-International notation, O_h^5-Schoenflies notation) shown in Fig. 2. This has the highest-symmetry point group

Table 1 Measurements and calculations of intrinsic birefringence of CaF_2 and BaF_2 in the UV.

Wavelength (nm)	CaF_2 $10^7\times(n_{\langle\bar{1}10\rangle} - n_{\langle 001\rangle})$		BaF_2 $10^7\times(n_{\langle\bar{1}10\rangle} - n_{\langle 001\rangle})$	
	Measured	Calculated	Measured	Calculated
365.06	0.19±0.04	0.66	4.0±0.6	5.3
253.65	−0.55±0.07	0.84	9.5±1.1	12.7
193.09	−3.4±0.2	−1.4	19±2	26.9
175.19	−5.7±0.3	−5.2	25±2	36.4
165.72	−8.3±0.4	−9.9	29±2	43.6
156.10	−11.8±0.4[a]	−19.7	34±3	52.7

[a]Interpolated value for CaF_2 at the excimer laser wavelength 157.63 nm is $\Delta n = (-11.2\pm0.4)\times10^{-7}$.

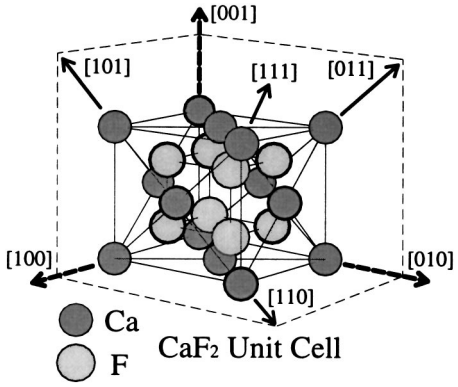

Fig. 2 Schematic of the conventional cubic unit cell of CaF_2, with the fluorite crystal structure. Ca atoms (dark circles on cube corners and faces) form a face-centered cubic lattice, and fluorine atoms (light circles on inside cube corners) form a simple cubic lattice. Directions in the crystal are indicated by the conventional notation with square brackets. The three orthogonal directions [100], [010], and [001] are parallel to the cube edges. The three orthogonal directions [110], [011], and [101] are parallel to the cube face diagonals. The direction [111] is parallel to a cube body diagonal (lower far corner to upper near corner).

possible for a crystal (crystal class: *m3m*-International notation, O_h-Schoenflies notation), with the full symmetry of a cube.[13] The 48 point group symmetry elements for this class consist of six distinguishable 90° rotations about the three fourfold rotation axes in the $\langle 100 \rangle$ directions (cube axes), three 180° rotations about these axes, six 180° rotations about the six twofold rotation axes in the $\langle 110 \rangle$ directions (cube face diagonals), eight 120° rotations about the four threefold rotation axes in the $\langle 111 \rangle$ directions (cube body diagonals), as well as the identity element and these elements combined with the inversion operation. Applying fourfold and twofold operations along two of the cubic axes of CaF_2 constrains $\epsilon_{ij}^{-1}(\omega,0)$ to have the form $\epsilon_{ij}^{-1}(\omega,0) = \epsilon^{-1}(\omega)\delta_{ij}$, where $\epsilon^{-1}(\omega)$ is a frequency-dependent scalar and δ_{ij} is the Kronecker δ. Thus for $\mathbf{q}=0$, $\epsilon_{ij}^{-1}(\omega,0)$ and the resulting optical properties are isotropic. This was the operating assumption of the optical designers using CaF_2 optical elements. However, for finite $\mathbf{q}$, this symmetry argument breaks down, and in general $\epsilon_{ij}^{-1}(\omega,\mathbf{q})$ gives birefringence and anisotropic indices. To determine this behavior we must determine the precise form of $\epsilon_{ij}^{-1}(\omega,\mathbf{q})$.

3.1 *Spatial Dispersion in Cubic Fluorite Structure Crystals*

Expanding the inverse dielectric tensor in a Taylor series expansion in $\mathbf{q}$ gives[14]

$$\epsilon_{ij}^{-1}(\omega,\mathbf{q}) = \epsilon^{-1}(\omega,0)\delta_{ij} + \sum_k \gamma_{ijk}(\omega) q_k + \sum_{kl} \beta_{ijkl}(\omega) q_k q_l + \ldots , \quad (2)$$

where $\epsilon^{-1}(\omega,0)$ is the isotropic inverse dielectric constant for $\mathbf{q}=0$, related to the $\mathbf{q}=0$ isotropic dielectric constant by $\epsilon^{-1}(\omega,0) = 1/\epsilon(\omega,0)$. (Note β in this paper is $-\epsilon(\omega,0)^{-2}\alpha$, for α from Ref. 3.) We expand the inverse dielectric tensor because it is directly related to the indices of refraction. Since CaF_2 is a centrosymmetric crystal (i.e., it has the inversion operation as a symmetry element), the coefficient γ_{ijk} of the term linear in q must vanish, as well as all terms with odd powers of q. The first correction to the isotropic inverse dielectric tensor is the term proportional to q^2, with tensor coefficient $\beta_{ijkl}(\omega)$ that determines the anisotropies and birefringence. Actually, for light that is introduced into a crystal, the value of q inside the crystal is scaled by a factor of the index n compared to what it would be in a vacuum, where n itself depends on $\sim q^2$ recursively through Eq. (2). These additional q-dependent terms affect $\epsilon_{ij}^{-1}(\omega,\mathbf{q})$ at fourth-order in q, which we neglect here.

The wavelength dependence of the q^2 term in Eq. (2) is roughly the square of the small parameter, an/λ, where a is the lattice constant and n is the index of refraction.[5] Consistent with the measured and calculated results shown in Fig. 1, the long-wavelength behavior is governed by the diminishing effect of the $1/\lambda^2$ term and by the totality of contributions to the anisotropic dielectric properties, e.g., band effects and exciton effects.[3] The divergent short-wavelength behavior is governed by the increasing character of $1/\lambda^2$ and especially by the strong contribution of the excitonic anisotropies near the band edge. If we consider the key case of CaF_2, $a=0.546$ nm, and for $\lambda=157$ nm, $n=1.56$, we have $(an/\lambda)^2 \sim 2.9\times 10^{-5}$. The next nonvanishing term in Eq. (2) goes as q^4, or in terms of the small parameter as $(an/\lambda)^4 \sim 8.7\times 10^{-10}$, which is small enough to justify the neglect of higher order terms at this wavelength.

Of course, for small enough λ, e.g., $\lambda \sim a$, Bragg scattering may occur, and the analysis presented here is not valid. Also, for photon energy sufficiently close to or above the crystal band gap energy or near impurity levels, the crystal has an absorption component and q becomes complex. This results in evanescence and an effective broadening of the real part of q. An evanescent component complicates the birefringence analysis based on propagating waves, and significant contributions from large q components may confound the conclusions drawn from the analysis based on a Taylor series expansion in a definite q out to the q^2 term. However, high-quality CaF_2 is sufficiently transmissive near 157 nm that these effects should not be concerns near this wavelength.

Equation (2) can be written as

$$\epsilon_{ij}^{-1}(\omega,\mathbf{q}) = \epsilon^{-1}(\omega,0)\delta_{ij} + \Delta\epsilon_{ij}^{-1}(\omega,\mathbf{q}), \quad (3)$$

where $\Delta\epsilon_{ij}^{-1}(\omega,\mathbf{q})$ is the anisotropic correction given to lowest order as

$$\Delta\epsilon_{ij}^{-1}(\omega,\mathbf{q}) = \sum_{kl} \beta_{ijkl}(\omega) q_k q_l . \quad (4)$$

$\beta_{ijkl}(\omega)$ is a fourth-rank matter tensor and must obey all the symmetry operations of the crystal. In general it has $3^4 = 81$ independent components, however symmetries put

constraints on the actual number of independent components. First, the symmetry of $\epsilon_{ij}^{-1}(\omega,\mathbf{q})$ and the product $q_k q_l$ show that $\beta_{ijkl}(\omega)$ is symmetric under interchanges $i\leftrightarrow j$ and $k\leftrightarrow l$. This reduces the 81 independent components to 36. A compressed matrix notation is convenient.[13] In $\beta_{ijkl}(\omega)$ the four indices $i=1-3$, $j=1-3$, $k=1-3$, $l=1-3$ can be replaced by two indices $i=1-6$, $j=1-6$ by making the associations

$$11\rightarrow 1,\ 22\rightarrow 2,\ 33\rightarrow 3,\ 23,32\rightarrow 4,\ 13,31\rightarrow 5 \quad \text{and} \quad 12,21\rightarrow 6. \tag{5}$$

Then all the independent components of the tensor $\beta_{ijkl}(\omega)$ can be written as a 6 by 6 matrix

$$\beta_{ijkl}(\omega)\leftrightarrow\beta_{ab}(\omega)$$

$$=\begin{pmatrix} \beta_{11} & \beta_{12} & \beta_{13} & \beta_{14} & \beta_{15} & \beta_{16} \\ \beta_{21} & \beta_{22} & \beta_{23} & \beta_{24} & \beta_{25} & \beta_{26} \\ \beta_{31} & \beta_{32} & \beta_{33} & \beta_{34} & \beta_{35} & \beta_{36} \\ \beta_{41} & \beta_{42} & \beta_{43} & \beta_{44} & \beta_{45} & \beta_{46} \\ \beta_{51} & \beta_{52} & \beta_{53} & \beta_{54} & \beta_{55} & \beta_{56} \\ \beta_{61} & \beta_{62} & \beta_{63} & \beta_{64} & \beta_{65} & \beta_{66} \end{pmatrix}_{ab}. \tag{6}$$

In practice, the matrix form relates $\Delta\epsilon_{ij}^{-1}(\omega,\mathbf{q})$ and $\mathbf{q}$ according to

$$\begin{pmatrix} \Delta\epsilon_{11}^{-1} \\ \Delta\epsilon_{22}^{-1} \\ \Delta\epsilon_{33}^{-1} \\ \Delta\epsilon_{23}^{-1} \\ \Delta\epsilon_{13}^{-1} \\ \Delta\epsilon_{12}^{-1} \end{pmatrix} = \begin{pmatrix} \beta_{11} & \beta_{12} & \beta_{13} & \beta_{14} & \beta_{15} & \beta_{16} \\ \beta_{21} & \beta_{22} & \beta_{23} & \beta_{24} & \beta_{25} & \beta_{26} \\ \beta_{31} & \beta_{32} & \beta_{33} & \beta_{34} & \beta_{35} & \beta_{36} \\ \beta_{41} & \beta_{42} & \beta_{43} & \beta_{44} & \beta_{45} & \beta_{46} \\ \beta_{51} & \beta_{52} & \beta_{53} & \beta_{54} & \beta_{55} & \beta_{56} \\ \beta_{61} & \beta_{62} & \beta_{63} & \beta_{64} & \beta_{65} & \beta_{66} \end{pmatrix} \times \begin{pmatrix} q_1^2 \\ q_2^2 \\ q_3^2 \\ 2q_2q_3 \\ 2q_1q_3 \\ 2q_1q_2 \end{pmatrix}. \tag{7}$$

(Technically this matrix form is not a tensor, because it does not have the coordinate transformation properties required of a tensor. By referring to the form as a tensor, we mean it as a short hand for the true fourth-rank tensor.)

Due to the symmetry operations of the crystal, various components are related. Using the symmetry operations B (threefold rotation about a cube body diagonal $\langle 111\rangle$), 2 (twofold rotation about a cube axis $\langle 001\rangle$), and 4 (fourfold rotation about a cube axis), it can be shown by direct inspection[15] that the only independent tensor components are β_{11}, β_{12}, and β_{44} (in the compressed notation), and the tensor has the form

$$\beta_{ijkl}(\omega)\leftrightarrow\beta_{ab}(\omega)$$

$$=\begin{pmatrix} \beta_{11} & \beta_{12} & \beta_{12} & 0 & 0 & 0 \\ \beta_{12} & \beta_{11} & \beta_{12} & 0 & 0 & 0 \\ \beta_{12} & \beta_{12} & \beta_{11} & 0 & 0 & 0 \\ 0 & 0 & 0 & \beta_{44} & 0 & 0 \\ 0 & 0 & 0 & 0 & \beta_{44} & 0 \\ 0 & 0 & 0 & 0 & 0 & \beta_{44} \end{pmatrix}_{ab}. \tag{8}$$

This has the same form as the piezo-optic tensor π_{ijkl} for CaF_2, which governs the effect of stress on the index, for the same symmetry reasons.[13] However, unlike the case of the piezo-optical effect, where stress can be applied in any direction and the index determined in any other direction, here the perturbing influence $\mathbf{q}$ has a definite relation (perpendicular) to an index direction, and this gives rise to further simplifications, as will be shown.

Because the components of a fourth-rank tensor transform like the product of the components of four vectors $\mathbf{V}_1$, $\mathbf{V}_2$, $\mathbf{V}_3$, and $\mathbf{V}_4$, the three linearly independent scalar combinations of the four vectors $(\mathbf{V}_1\cdot\mathbf{V}_2)(\mathbf{V}_3\cdot\mathbf{V}_4)$, $(\mathbf{V}_1\cdot\mathbf{V}_3)(\mathbf{V}_2\cdot\mathbf{V}_4)$, and $(\mathbf{V}_1\cdot\mathbf{V}_4)(\mathbf{V}_2\cdot\mathbf{V}_3)$ imply that a fourth-rank tensor has three scalar invariants (independent combinations of tensor components that are invariant under coordinate transformations.)[15] Since $\beta_{ijkl}(\omega)$ is symmetric on interchange of the first two and last two indices, the second and third scalar invariants are equivalent, and thus $\beta_{ijkl}(\omega)$ has two isotropic scalar invariants

$$J_1(\omega)=\frac{1}{3}\sum_{ij}\beta_{iijj}=\beta_{11}+2\beta_{12}, \tag{9}$$

$$J_2(\omega)=\frac{1}{3}\sum_{ij}\beta_{ijij}=\beta_{11}+2\beta_{44}. \tag{10}$$

The existence of the isotropic scalar invariants motivates us to write Eq. (8) as

$$\beta_{ab}(\omega)=\beta_{ab}(\omega)^{\text{isotropic}'}+\beta_{ab}(\omega)^{\text{longitudinal}'}+\beta_{ab}(\omega)^{\text{anisotropic}'} \tag{11}$$

with

$$\beta_{ab}(\omega)^{\text{isotropic}'}=I_1(\omega)\begin{pmatrix} 1 & 1 & 1 & 0 & 0 & 0 \\ 1 & 1 & 1 & 0 & 0 & 0 \\ 1 & 1 & 1 & 0 & 0 & 0 \\ 0 & 0 & 0 & 0 & 0 & 0 \\ 0 & 0 & 0 & 0 & 0 & 0 \\ 0 & 0 & 0 & 0 & 0 & 0 \end{pmatrix}_{ab}, \tag{12}$$

$$\beta_{ab}(\omega)^{\text{longitudinal}'} = I_2(\omega)\begin{pmatrix} 2 & 0 & 0 & 0 & 0 & 0 \\ 0 & 2 & 0 & 0 & 0 & 0 \\ 0 & 0 & 2 & 0 & 0 & 0 \\ 0 & 0 & 0 & 1 & 0 & 0 \\ 0 & 0 & 0 & 0 & 1 & 0 \\ 0 & 0 & 0 & 0 & 0 & 1 \end{pmatrix}_{ab}, \tag{13}$$

$$\beta_{ab}(\omega)^{\text{anisotropic}'} = A(\omega)\begin{pmatrix} 2 & -1 & -1 & 0 & 0 & 0 \\ -1 & 2 & -1 & 0 & 0 & 0 \\ -1 & -1 & 2 & 0 & 0 & 0 \\ 0 & 0 & 0 & -1 & 0 & 0 \\ 0 & 0 & 0 & 0 & -1 & 0 \\ 0 & 0 & 0 & 0 & 0 & -1 \end{pmatrix}_{ab}. \tag{14}$$

The new variables $I_1 \equiv (2J_1 - J_2)/5$, $I_2 \equiv (-J_1 + 3J_2)/10$, and A are linear combinations of β_{11}, β_{12}, and β_{44}

$$\begin{pmatrix} I_1 \\ I_2 \\ A \end{pmatrix} = \frac{1}{5}\begin{pmatrix} 1 & 4 & -2 \\ 1 & -1 & 3 \\ 1 & -1 & -2 \end{pmatrix}\begin{pmatrix} \beta_{11} \\ \beta_{12} \\ \beta_{44} \end{pmatrix} \tag{15}$$

or equivalently

$$\begin{pmatrix} \beta_{11} \\ \beta_{12} \\ \beta_{44} \end{pmatrix} = \begin{pmatrix} 1 & 2 & 2 \\ 1 & 0 & -1 \\ 0 & 1 & -1 \end{pmatrix}\begin{pmatrix} I_1 \\ I_2 \\ A \end{pmatrix}. \tag{16}$$

The new variables I_1, I_2, and A have physical interpretations. Using Eqs. (12)–(14) in Eq. (4), going back to the uncompressed notation, and summing over the q's using Eq. (7), then $\Delta\epsilon_{ij}^{-1}(\omega,\mathbf{q})$ can be written as

$$\Delta\epsilon_{ij}^{-1}(\omega,\mathbf{q}) = \Delta\epsilon_{ij}^{-1}(\omega,\mathbf{q})^{\text{isotropic}'} + \Delta\epsilon_{ij}^{-1}(\omega,\mathbf{q})^{\text{longitudinal}'} + \Delta\epsilon_{ij}^{-1}(\omega,\mathbf{q})^{\text{anisotropic}'} \tag{17}$$

with

$$\Delta\epsilon_{ij}^{-1}(\omega,\mathbf{q})^{\text{isotropic}'} = I_1(\omega)q^2\begin{bmatrix} 1 & 0 & 0 \\ 0 & 1 & 0 \\ 0 & 0 & 1 \end{bmatrix}_{ij} = I_1(\omega)q^2\delta_{ij}, \tag{18}$$

$$\Delta\epsilon_{ij}^{-1}(\omega,\mathbf{q})^{\text{longitudinal}'} = I_2(\omega)2q^2\begin{bmatrix} l_1^2 & l_1l_2 & l_1l_3 \\ l_2l_1 & l_2^2 & l_2l_3 \\ l_3l_1 & l_3l_2 & l_3^2 \end{bmatrix}_{ij} = I_2(\omega)2q^2 l_i l_j, \tag{19}$$

$$\Delta\epsilon_{ij}^{-1}(\omega,\mathbf{q})^{\text{anisotropic}'} = A(\omega)q^2\begin{bmatrix} 3l_1^2-1 & -2l_1l_2 & -2l_1l_3 \\ -2l_2l_1 & 3l_2^2-1 & -2l_2l_3 \\ -2l_3l_1 & -2l_3l_2 & 3l_3^2-1 \end{bmatrix}_{ij} = A(\omega)q^2(\delta_{ij}(5l_i^2-1) - 2l_il_j), \tag{20}$$

where l_1, l_2, l_3 are the direction cosines of the x_1, x_2, x_3 axes, respectively.

$\Delta\epsilon_{ij}^{-1}(\omega,\mathbf{q})^{\text{isotropic}'} \propto I_1\delta_{ij}$ gives an isotropic shift in the inverse dielectric tensor, and therefore cannot contribute to any anisotropic effects. Moreover, because $\Delta\epsilon_{ij}^{-1}(\omega,\mathbf{q})^{\text{isotropic}'}$ has the same angular dependence as $\epsilon^{-1}(\omega,0)\delta_{ij}$ from Eq. (3), it is not a practicable observable.

$\Delta\epsilon_{ij}^{-1}(\omega,\mathbf{q})^{\text{longitudinal}'} \propto I_2 l_i l_j$ gives a shift in the dielectric tensor for the directions of propagation and polarization aligned. For example, for propagation along the x_3 axis, $l_1=0$, $l_2=0$, and $l_3=1$, giving

$$\Delta\epsilon_{ij}^{-1}(\omega,q\hat{\mathbf{x}}_3)^{\text{longitudinal}} = I_2(\omega)2q^2\begin{bmatrix} 0 & 0 & 0 \\ 0 & 0 & 0 \\ 0 & 0 & 1 \end{bmatrix}_{ij}. \tag{21}$$

Because the propagating waves are polarized in the transverse plane—the x_1, x_2 plane in this example—this term has no effect on the bulk optical properties.

The optical manifestations of the anisotropy are all contained in $\Delta\epsilon_{ij}^{-1}(\omega,\mathbf{q})^{\text{anisotropic}'}$. Thus while the cubic crystal supports three independent tensor components, only one combination is relevant to anisotropies. This conclusion is central to the present paper. Although I_1 and I_2 exist physically, they have no practical observable consequences in optics. Hence it is permissible to ignore I_1 and I_2 when considering the anisotropic optical behavior and birefringence.

Note that the form for $\Delta\epsilon_{ij}^{-1}(\omega,\mathbf{q})^{\text{anisotropic}'}$ obtained above by setting the scalar invariants to zero is a traceless combination of three terms. The second and third terms of $\Delta\epsilon_{ij}^{-1}(\omega,\mathbf{q})^{\text{anisotropic}'}$ in Eq. (20) are proportional to δ_{ij} and l_il_j, respectively, which again give only isotropic and purely longitudinal contributions. These terms can be subsumed into the isotropic and longitudinal terms in Eq. (17) giving

$$\Delta\epsilon_{ij}^{-1}(\omega,\mathbf{q})=\Delta\epsilon_{ij}^{-1}(\omega,\mathbf{q})^{\text{isotropic}}+\Delta\epsilon_{ij}^{-1}(\omega,\mathbf{q})^{\text{longitudinal}}+\Delta\epsilon_{ij}^{-1}(\omega,\mathbf{q})^{\text{anisotropic}} \tag{22}$$

$$=[I_1(\omega)-A(\omega)]q^2\delta_{ij}+[I_2(\omega)-A(\omega)]2q^2l_il_j+A(\omega)5q^2\delta_{ij}l_i^2. \tag{23}$$

Just as before, the first term may be considered as an unobservable shift in the dielectric constant, and we can ignore it. The second term does not affect propagating waves, so we can also ignore it. We need to consider only the third term. It gives a pure anisotropic contribution and has the form

$$\Delta\epsilon_{ij}^{-1}(\omega,\mathbf{q})^{\text{anisotropic}}=A(\omega)5q^2\begin{bmatrix}l_1^2 & 0 & 0\\ 0 & l_2^2 & 0\\ 0 & 0 & l_3^2\end{bmatrix}_{ij}$$

$$=A(\omega)5q^2\delta_{ij}l_i^2. \tag{24}$$

The corresponding β_{ab} tensor in the compressed form appropriate to Eqs. (4) and (11) is

$$\beta_{ab}(\omega)^{\text{anisotropic}}=A(\omega)5\begin{pmatrix}1&0&0&0&0&0\\0&1&0&0&0&0\\0&0&1&0&0&0\\0&0&0&0&0&0\\0&0&0&0&0&0\\0&0&0&0&0&0\end{pmatrix}_{ab}. \tag{25}$$

This governs, in a pure form, all the anisotropies and birefringence resulting from spatial dispersion up to order q^2 in the expansion Eq. (2). Remarkably, the form of Eq. (25) gives precisely the same results for the angle dependence as that of Eq. (14) and Eq. (8). Despite the three independent coefficients in Eq. (8) allowed by symmetry, the anisotropies are in fact proportional to just one parameter, namely $A(\omega)=(\beta_{11}-\beta_{12}-2\beta_{44})/5$. This simplification occurs essentially because **q** always determines the direction of the symmetry-breaking perturbation. Equation (25) has a deceptively innocent-looking form. However, it gives rise to complex, though highly symmetric, anisotropic behavior with diverse consequences, which we discuss next.

3.2 *Birefringence and Index Anisotropy*

Knowing the inverse dielectric tensor $\epsilon_{ij}^{-1}(\omega,\mathbf{q})$ for a CaF_2 crystal for all propagation directions, we may obtain the indices of refraction. We review the prescription for this.[13,16] From the sourceless Maxwell equations in nonmagnetic materials ($\text{curl}\mathbf{H}=1/c\,\partial\mathbf{D}/\partial t$, $\text{curl}\mathbf{E}=-1/c\,\partial\mathbf{B}/\partial t$, and $\mathbf{B}=\mathbf{H}$), for a plane wave $\sim e^{i(\mathbf{q}\cdot\mathbf{r}-\omega t)}$ propagating with angular frequency ω and wave vector **q**, it is straightforward to show that the electric field **E** and the electric displacement field **D** are related by the equation

$$(v/c)^2\mathbf{D}=\mathbf{E}-(\hat{\mathbf{q}}\cdot\mathbf{E})\hat{\mathbf{q}}, \tag{26}$$

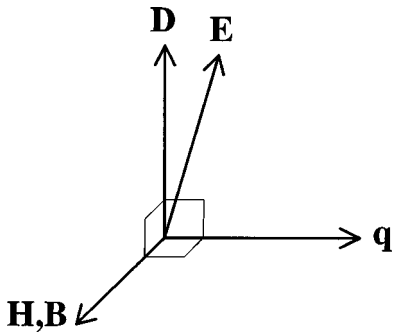

Fig. 3 Relation between the directions of the **B**, **H**, **E**, **D**, and **q** vectors for light propagation in anisotropic, nonmagnetic crystals. **H**, **D**, and **q** are mutually perpendicular. **D**, **E**, and **q** are coplanar.

where v is the velocity of the wave front along the wave normal $\hat{\mathbf{q}}=\mathbf{q}/|\mathbf{q}|$. From the Maxwell equations, **D**, **H**, and **q** must be mutually perpendicular and **E** must be in the plane of **q** and **D**, as shown in Fig. 3.

Choose a coordinate system with one axis along $\hat{\mathbf{q}}$ and the two mutually perpendicular transverse axes arbitrary, with components along these axes labeled α and β. Then from Eq. (26), the **D** and **E** components along these axes are given by

$$D_\alpha=(c/v)^2E_\alpha=n^2E_\alpha \quad (n\equiv c/v), \tag{27}$$

where $n\equiv c/v$ is the index of refraction.

Using Eq. (1) for E_α and the fact that **D** must be perpendicular to $\hat{\mathbf{q}}$, the following relation must hold between the components of **D** and the index of refraction n

$$\sum_\beta\left(\epsilon_{\alpha\beta}^{-1}-\frac{1}{n^2}\delta_{\alpha\beta}\right)D_\beta=0. \tag{28}$$

A nonzero solution requires that the determinant of the coefficients of D_β be zero, allowing two possible values for $1/n^2$. These are given by the two eigenvalues $\epsilon_\gamma^{-1\perp}=\epsilon_1^{-1\perp},\epsilon_2^{-1\perp}$ of $\epsilon_{\alpha\beta}^{-1}$, obtained as above by diagonalization of ϵ_{ij}^{-1} in the plane transverse to $\hat{\mathbf{q}}$. Plane waves propagating in the crystal must be completely linearly polarized with the two possible polarization directions of **D** determined by the two eigenvectors of Eq. (28). The indices of refraction of the two polarization states are given by

$$n_\gamma=\sqrt{1/\epsilon_\gamma^{-1\perp}}. \quad (\gamma\rightarrow 1,2\text{-the eigenvalues of } \epsilon_{\alpha\beta}^{-1}). \tag{29}$$

Thus to determine the index properties of CaF_2, we need to find the eigenvalues of ϵ_{ij}^{-1} projected into the plane transverse to **q**.

From Eqs. (3), (22), and (23), the dielectric tensor required in Eq. (29) is given by

$$\epsilon_{ij}^{-1}(\omega,\mathbf{q})=(\epsilon^{-1}(\omega,0)+(I_1(\omega)-A(\omega))q^2)\delta_{ij}+A(\omega)5q^2\delta_{ij}l_i^2, \tag{30}$$

where we have ignored the longitudinal terms because they cannot affect the transverse eigenvalues. The two eigenvalues of $\epsilon_{ij}^{-1}(\mathbf{q},\omega)$ in the plane transverse to $\mathbf{q}$ are given by

$$\epsilon_{\gamma}^{-1\perp}=(\epsilon^{-1}(\omega,0)+(I_1(\omega)-A(\omega))q^2) +A(\omega)5q^2\mathrm{EigVal}(\delta_{ij}l_i^2)_{\gamma}^{\perp} \quad (\gamma=1,2), \tag{31}$$

where $\mathrm{EigVal}(\delta_{ij}l_i^2)_{\gamma}^{\perp}$ is one of the two eigenvalues of the tensor $(\delta_{ij}l_i^2)$ in the plane transverse to $\mathbf{q}$. Using these in Eq. (29) gives the indices of refraction for the two polarization states

$$n_{\gamma}=[(\epsilon^{-1}(\omega,0)+(I_1(\omega)-A(\omega))q^2) +A(\omega)5q^2\mathrm{EigVal}(\delta_{ij}l_i^2)_{\gamma}^{\perp}]^{-1/2} \quad (\gamma=1,2). \tag{32}$$

This is exact to order q^2 in the expansion Eq. (2).

Since the first term in the square root in Eq. (32) is of order 1 and the terms proportional to q^2 are, from measurements shown in Table 1, of order $\sim 10^{-6}$, then for wavelengths down to at least 157 nm, the square root in Eq. (32) can be expanded to very high accuracy. Using $\epsilon^{-1}(\omega,0)=1/\epsilon(\omega,0)=1/n(\omega,0)^2$, where $n(\omega,0)$ is the isotropic index of refraction at frequency ω for $\mathbf{q}=0$, and using Eq. (15) for I_1 and A, we finally get to order q^2

$$n_{\gamma}(\omega,\mathbf{q})=n(\omega,0)-\tfrac{1}{2}n(\omega,0)^3\beta_{12}q^2-\tfrac{1}{2}n(\omega,0)^3 \times(\beta_{11}-\beta_{12}-2\beta_{44})q^2\mathrm{EigVal}(\delta_{ij}l_i^2)_{\gamma}^{\perp}+O(q^4). \tag{33}$$

Thus the propagation direction dependence of the two indices for the two orthogonal polarization states of light traveling in a fluorite-structure crystal with spatial dispersion, is given by the eigenvalues of $(\delta_{ij}l_i^2)$ in the plane transverse to $\mathbf{q}$.

From Eq. (33), the birefringence is given by

$$\Delta n(\omega,\mathbf{q})=[n_1(\omega,\mathbf{q})-n_2(\omega,\mathbf{q})] =-\tfrac{1}{2}n(\omega,0)^3(\beta_{11}-\beta_{12}-2\beta_{44})q^2 \times[\mathrm{EigVal}(\delta_{ij}l_i^2)_1^{\perp}-\mathrm{EigVal}(\delta_{ij}l_i^2)_2^{\perp}]+O(q^4). \tag{34}$$

The variation of the birefringence with propagation direction is fully determined by the angular dependence of the eigenvalue difference, which is calculated in Sec. 3.4. The same angular dependence occurs for all fluorite-structure crystals at all wavelengths in the range of validity of the model, discussed in Sec. 3.1. The magnitude is governed by the factor $(n(\omega,0)^3(\beta_{11}-\beta_{12}-2\beta_{44})q^2)$, which is a constant for a given material and wavelength. Thus the full behavior of the intrinsic birefringence for a given material at a given wavelength is determined by a single birefringence measurement.

The average of the indices for the two polarization states for propagation with a wave vector $\mathbf{q}$ is given by

$$n(\omega,\mathbf{q})^{\mathrm{Av}}=\tfrac{1}{2}[n_1(\omega,\mathbf{q})+n_2(\omega,\mathbf{q})] =n(\omega,0)-\tfrac{1}{2}n(\omega,0)^3\beta_{12}q^2-\tfrac{1}{4}n(\omega,0)^3 \times(\beta_{11}-\beta_{12}-2\beta_{44})q^2[\mathrm{EigVal}(\delta_{ij}l_i^2)_1^{\perp} +\mathrm{EigVal}(\delta_{ij}l_i^2)_2^{\perp}]+O(q^4). \tag{35}$$

The variation with propagation direction is fully determined by the angular dependence of the eigenvalue sum, calculated in Sec. 3.4. The magnitude of the variation is determined by the same material parameter combination as for the birefringence, so the full behavior of the index variation is also determined for a given material at a given wavelength by a single birefringence measurement. The absolute average index value is determined by a combination of the large, q independent, isotropic band effects and the small spatial-dispersion effects, which are difficult to distinguish experimentally.

Note that when we have $(\beta_{11}-\beta_{12}-2\beta_{44})=0$, the optical properties are completely isotropic. In principle, nothing prevents this condition from being met in a real material at a particular wavelength, for example, in a cubic-fluorite-structure crystal formed as a mixed solid solution.[8]

3.3 *Eigenvalues of the Anisotropic Inverse Dielectric Tensor*

To obtain the indices we must determine the eigenvalues and eigenvectors in the plane transverse to $\mathbf{q}$ for

$$\Delta\epsilon_{ij}^{-1}(\omega,\mathbf{q})^{\mathrm{anisotropic}}=(A(\omega)5q^2)\begin{bmatrix}l_1^2&0&0\\0&l_2^2&0\\0&0&l_3^2\end{bmatrix}_{ij} =(A(\omega)5q^2)(\delta_{ij}l_i^2). \tag{36}$$

We will first consider propagation in three special directions, and then we find the solution for the general direction. First consider the propagation direction along the cube axis direction [001]. Evaluating the direction cosines l_i in Eq. (36) $(l_1=0,\ l_2=0,\ l_3=1)$ gives

$$\Delta\epsilon_{ij}^{-1}(\omega,\hat{\mathbf{q}}^{001})^{\mathrm{anisotropic}}=(A(\omega)5q^2)\begin{bmatrix}0&0&0\\0&0&0\\0&0&1\end{bmatrix}_{ij}. \tag{37}$$

This is trivially diagonal and uniaxial with the axis in the propagation direction. The transverse eignenvalues are both 0. There is no birefringence for propagation along this axis or equivalent $\langle 001\rangle$ axes.

Now consider the propagation direction along the cube body diagonal direction [111]. Evaluating the direction cosines l_i in Eq. (36) $(l_1=l_2=l_3=1/\sqrt{3})$ gives

$$\Delta\epsilon_{ij}^{-1}(\omega,\hat{\mathbf{q}}^{111})^{\mathrm{anisotropic}}=(A(\omega)5q^2)\frac{1}{3}\begin{bmatrix}1&0&0\\0&1&0\\0&0&1\end{bmatrix}_{ij}. \tag{38}$$

This is the isotropic tensor, with all eigenvalues equal to 1/3, ignoring the $(A(\omega)5q^2)$ factor for the moment. There is also no birefringence for propagation along this axis or equivalent $\langle 111\rangle$ axes.

These two results are also apparent from symmetry alone, since a uniaxial perturbation ($\mathbf{q}$) along a fourfold or threefold axis in a cubic crystal reduces the isotropic symmetry to uniaxial along the axis, so both these axes must be nonbirefringent. However, note that the transverse eigenvalues for the $\langle 001\rangle$ directions and the $\langle 111\rangle$ directions, 0 and 1/3, respectively, are not equal. This means that the indices for propagation in these nonbirefringent directions are not equal. Indeed, these values of the index are the extremal values for all directions.

Finally, consider the propagation direction along the cube face diagonal direction [110]. Evaluating the direction cosines l_i in Eq. (36) ($l_1=l_2=1/\sqrt{2}$, $l_3=0$) gives

$$\Delta\epsilon_{ij}^{-1}(\omega,\hat{\mathbf{q}}^{110})^{\text{anisotropic}}=(A(\omega)5q^2)\frac{1}{2}\begin{bmatrix}1&0&0\\0&1&0\\0&0&0\end{bmatrix}_{ij}. \quad (39)$$

This is a bit more work, but not much. We need to diagonalize in the plane orthogonal to the direction [110]. The eigenvectors must therefore be some linear combination of the two vectors [1$\bar{1}$0] and [001], since these are orthogonal to [110] and to each other. They are, in fact, the transverse eigenvectors

$$\text{Eigenvectors:}\quad \begin{bmatrix}-1\\1\\0\end{bmatrix}\quad\begin{bmatrix}0\\0\\1\end{bmatrix}\quad\begin{bmatrix}1\\1\\0\end{bmatrix}. \quad (40)$$

$$\begin{array}{lccc}\text{Eigenvalues} & 1/2 & 0 & 1/2\\ & \text{transverse} & \text{transverse} & \text{longitudinal}\end{array}. \quad (41)$$

The transverse eigenvectors, and thus the polarization eigenstates, are along the [$\bar{1}$10] and the [001] axes. It can be shown that the $\langle 110\rangle$ propagation directions are the directions of maximum eigenvalue difference (maximum birefringence).

The two transverse eigenvalues are split by a value 1/2, which gives rise to the birefringence. The actual magnitude and sign of the birefringence is determined using Eq. (34) by $(n_{\langle\bar{1}10\rangle}(\omega,\mathbf{q})-n_{\langle 001\rangle}(\omega,\mathbf{q}))=-(1/4)n(\omega,0)^3(\beta_{11}-\beta_{12}-2\beta_{44})q^2$. The [$\bar{1}$10] axis is the low index (fast) axis if we have $(\beta_{11}-\beta_{12}-2\beta_{44})>0$. This is what is observed for CaF_2 at short wavelength, as shown in Table 1 and Fig. 1. (BaF_2 has the opposite sign.) However, as shown in the table and figure, there is a sign change for CaF_2 determined by both measurement and calculation for wavelengths below $\sim$200 nm.

This analysis applies to the three cubic crystal classes (*432*, $\bar{4}3m$, and *m3m*-International notation; *O*, T_d, O_h-Schoenflies notation) that contain fourfold symmetry axes. The two other cubic crystal classes (*23* and *m3*, *T* and T_h), which do not contain fourfold symmetry axes, have a fourth material parameter β_{13} that complicates the picture.

3.4 *Directional Dependence of the Birefringence and Index Anistropy*

To find the indices for a general propagation direction $\hat{\mathbf{q}}$, the tensor $M_{ij}\equiv\delta_{ij}l_i^2$ from Eq. (36) must be diagonalized in the plane transverse to $\hat{\mathbf{q}}$ as discussed in Sec. 3.2. Fairly simple closed-form solutions may be obtained analytically. To obtain these, one constructs the mutually orthogonal unit vectors $\hat{\theta}$ and $\hat{\phi}$ orthogonal to $\hat{\mathbf{q}}$, and projects the tensor into the two-dimensional subspace of $\hat{\theta}$ and $\hat{\phi}$, by forming the inner products of M_{ij} with the components of $\hat{\theta}$ and $\hat{\phi}$, e.g., $\mu_{11}=\Sigma_{ij}M_{ij}\hat{\theta}_i\hat{\theta}_j$, $\mu_{12}=\mu_{21}=\Sigma_{ij}M_{ij}\hat{\theta}_i\hat{\phi}_j$, $\mu_{22}=\Sigma_{ij}M_{ij}\hat{\phi}_i\hat{\phi}_j$. Then one solves for the eigenvalues of the 2 by 2 matrix. The solutions are the two roots of a quadratic equation. Finally, the polarization eigenstates are obtained by projecting the eigenvectors of the 2 by 2 matrix back into the Cartesian space. An explicit solution in terms of spherical coordinates $x_1=\sin\theta\cos\phi$, $x_2=\sin\theta\sin\phi$, $x_3=\cos\theta$ is given by

$$\text{EigVal}(\delta_{ij}l_i^2)_{1,2}^{\perp}=F(\theta,\phi)\pm G(\theta,\phi), \quad (42)$$

$$F(\theta,\phi)=\tfrac{1}{320}[-9-20\cos(2\theta)-35\cos(4\theta)-40\cos(4\phi)\sin^4(\theta)]+\tfrac{1}{5}, \quad (43)$$

$$G(\theta,\phi)=[\tfrac{1}{8}[5+3\cos(4\phi)]\cos^4(\theta)\sin^4(\theta)-\cos^2(\phi)\cos^2(\theta)\sin^2(\phi)\sin^6(\theta)+\cos^4(\phi)\sin^4(\phi)\sin^8(\theta)]^{1/2}. \quad (44)$$

The last term $+(1/5)$ in $F(\theta,\phi)$ is the eigenvalue shift resulting from removing the isotropic component from Eq. (20), and does not affect the birefringence or anisotropy.

This can be written more compactly using the direction cosines of $\hat{\mathbf{q}}$ with respect to the x_1,x_2,x_3 axes, l_1,l_2,l_3, related to the spherical coordinates by $l_1=\sin\theta\cos\phi$, $l_2=\sin\theta\sin\phi$, and $l_3=\cos\theta$. Then the solution can be written

$$\text{EigVal}(\delta_{ij}l_i^2)_{1,2}^{\perp}=F'(l_1,l_2,l_3)\pm G'(l_1,l_2,l_3), \quad (45)$$

$$F'(l_1,l_2,l_3)=(1/2)(1-l_1^4-l_2^4-l_3^4), \quad (46)$$

$$G'(l_1,l_2,l_3)=[(l_1^2l_2^2+l_2^2l_3^2+l_3^2l_1^2)^2-3l_1^2l_2^2l_3^2]^{1/2}. \quad (47)$$

This form, written using direction cosines, transparently reveals the cubic symmetry of the effects.

The variation of the average index with propagation direction is governed by

$$[\text{EigVal}(\delta_{ij}l_i^2)_1^{\perp}+\text{EigVal}(\delta_{ij}l_i^2)_2^{\perp}](1/2)=F'(l_1,l_2,l_3). \quad (48)$$

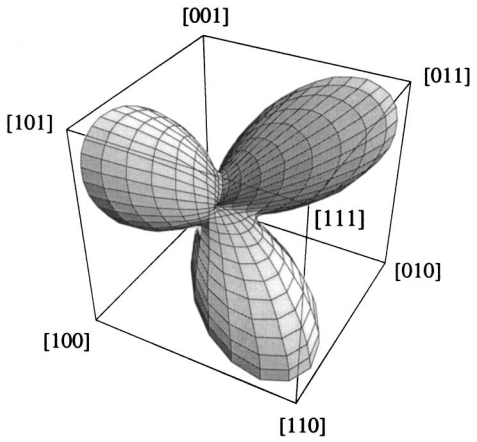

Fig. 4 The angular dependence of the intrinsic birefringence for propagation directions in one octant of a sphere. Directions refer to crystallographic directions indicated in square brackets. The magnitude of the birefringence in a given direction is proportional to the distance of the surface in that direction from the origin, with the maximum scaled to 1. A VRML (Virtual Reality Modeling Language) version may be found in Ref. 8.

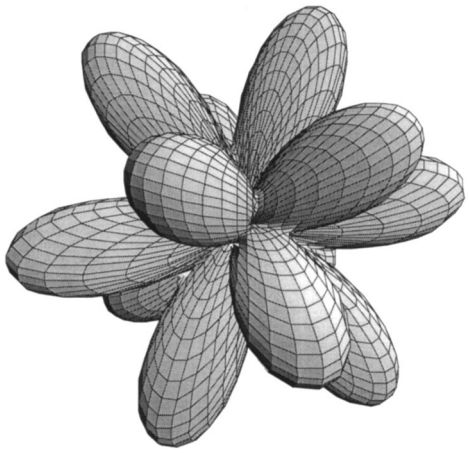

Fig. 5 Three-dimensional directional dependence of the intrinsic birefringence from a perspective along a general low-symmetry direction shows 12 birefringence maxima directions and 14 birefringence zero directions (seven nonbirefringent axes).

The variation of the birefringence with propagation direction is governed by

$$[\mathrm{EigVal}(\delta_{ij}l_i^2)_1^{\perp} - \mathrm{EigVal}(\delta_{ij}l_i^2)_2^{\perp}] = 2G'(l_1,l_2,l_3). \qquad (49)$$

A plot of the magnitude of the difference between the two eigenvalues (proportional to the birefringence) is shown in Fig. 4 for directions in one octant of a sphere. It indicates the birefringence (scaled to 1 at the maximum) for a given propagation direction, by the distance of the surface from the origin in that direction. The figure shows birefringence zeros in the ⟨100⟩ directions (cube axes) and in the ⟨111⟩ directions (cube body diagonals) as discussed in Sec. 3.3. A maximum occurs in the [110] direction (cube face diagonal), with the two polarization directions in the face diagonal $[\bar{1}10]$ and cube axes [001] directions. The ⟨110⟩ directions are the directions of absolute extrema in birefringence. Near these directions the birefringence falls off isotropically. The behavior in the other octants is equivalent by symmetry.

The complexity and high symmetry of the birefringence is demonstrated in the three-dimensional (3D) plot in Fig. 5. There are 12 directions of birefringence maxima, in the directions of the 12 cube edge centers. There are 14 directions of birefringence zero, along the three cube axes and the four cube body diagonals. In conventional optics (i.e., ignoring spatial dispersion), crystals are classified as either isotropic, uniaxial (1 nonbirefringent axis), or biaxial (2 nonbirefringent axes); however, optics including spatial-dispersion effects must treat cubic crystals (with the symmetry classes *432*, $\bar{4}3m$, and *m3m*) as *heptaxial* (seven nonbirefringent axes). Further, whereas in biaxial crystals the two nonbirefringent axes have the same index values, in this case the index for the four ⟨111⟩ nonbirefringent axes differs from the index for the three ⟨100⟩ axes.

The behavior of the birefringence, scaled to 1 at the maximum, in a cube diagonal plane is shown in Fig. 6, along with the average index. The figure shows that the birefringence (index out-of-plane minus index in-plane) has a maximum in magnitude in the [110] direction. The figure also shows a secondary birefringence maximum magnitude between the [001] and [111] directions. This occurs in the [211] direction, and, in fact, is a saddle point. A sign change occurs as the propagation direction passes through the [111] direction. The slope is nearly maximal at the zero crossing. Three gradient maxima occur very near each ⟨111⟩ direction. The average index curve shows that the average index variation is about as large in magnitude as the birefringence, and that the extremes occur in the directions of the birefringence zeros. A similar set of plots for propagation in the plane of a cube face is shown in Fig. 7. We verified this angle dependence by experiment, as shown in Fig. 8.

Another useful way to visualize the birefringence and index anisotropy is with index surfaces, which represent the

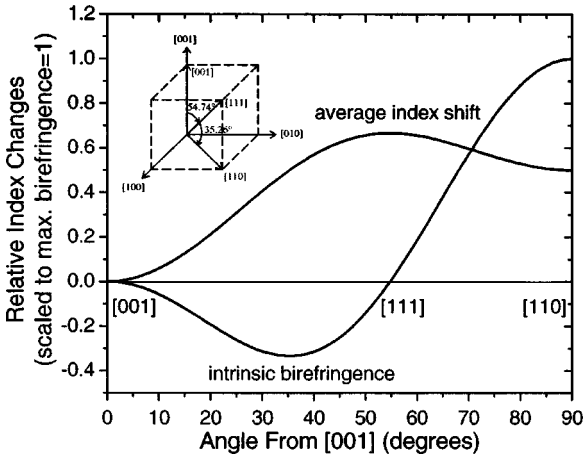

Fig. 6 Calculated magnitudes of the intrinsic birefringence (normalized to 1 at the maximum) and the average index shift, for propagation in directions in the cube diagonal plane $(\bar{1}10)$ containing the [001], [111], and [110] directions, represented by the angle measured from the [001] direction. The birefringence plotted is proportional to the index of refraction for the polarization normal to the $(\bar{1}10)$ plane, minus the index for the polarization in the $(\bar{1}10)$ plane.

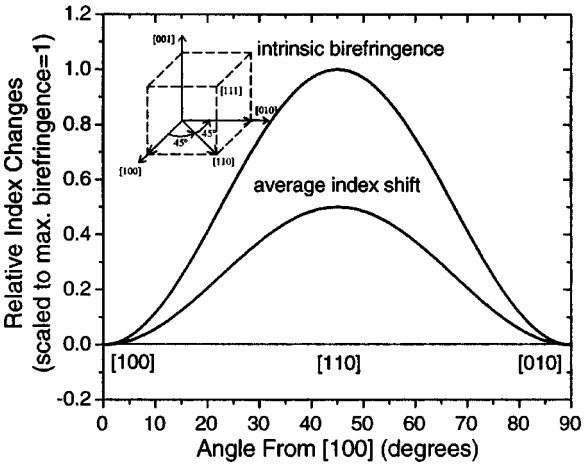

Fig. 7 Calculated magnitudes of the intrinsic birefringence (normalized to 1 at the maximum) and the average index shift, for propagation in directions in the cube face (001) plane containing the [100], [110], and [010] directions, represented by the angle measured from the [100] direction.

two indices for each propagation direction by two nested surfaces. For the case of cubic crystals with spatial dispersion, the index surfaces are much more complicated objects than those for biaxial crystals without spatial dispersion. The resulting ''nested lumpy spheres'' are shown in Fig. 9, with the anisotropy scaled to large values for visualization. Slices through these index surfaces for propagation in the $(\bar{1}10)$ plane and (001) plane plane are shown in Figs. 10 and 11 (cf. Figs. 6 and 7).

Plots of the eigenvectors are also illuminating. Figure 12 shows the eigenvector directions (polarization directions) for the larger index eigenvalues (slow axes), for propagation directions in an octant of a sphere. The magnitude of the polarization vector is scaled to the value of the birefringence for each propagation direction. Consistent with Figs. 6 and 10, the figure shows that sweeping the propagation

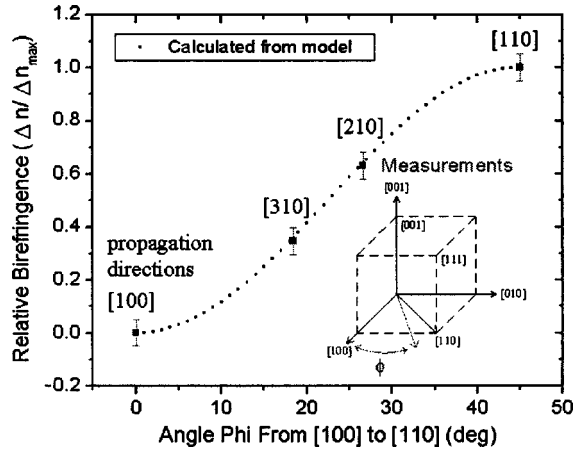

Fig. 8 Angular dependence of the intrinsic birefringence scaled to 1 at the maximum. Measured data (large squares with error bars) and model results (small squares) given for propagation directions in the (001) plane at the angle ϕ from the [100] direction, as indicated in the inset (Ref. 2). Measured results verify the model for the angular dependence given in Eqs. (44) and (47).

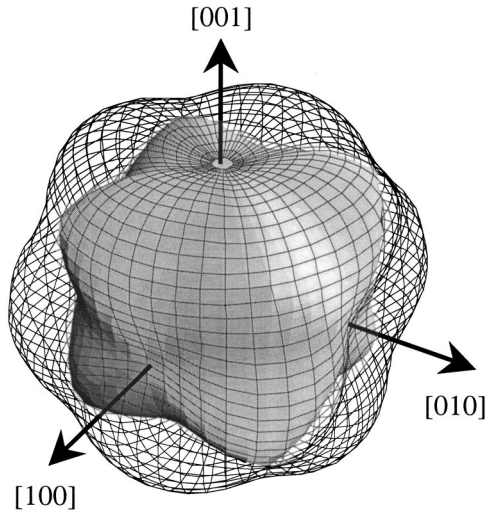

Fig. 9 Index surfaces for intrinsic birefringence in cubic fluorite-structure crystals. The indices for each of the two polarization eigenstates for each propagation direction are represented by the distance from the origin of a continuous and a wire mesh surface. The anisotropy is scaled to large values for visualization. The surfaces touch in the 14 nonbirefringent directions. Plane slices through the surfaces are shown in Figs. 10 and 11.

direction in the diagonal plane $(\bar{1}10)$, starting with propagation in the [001] direction, the magnitude of the index difference increases from zero, with the in-plane polarization index larger. The indices are equal again in the [111] direction, after which the larger index polarization direction switches to the out-of-plane direction. The difference reaches a maximum in the [110] direction. The figure assumes $(n_{\langle\bar{1}10\rangle} - n_{\langle 001\rangle})$ is positive. For CaF_2 near 157 nm the value is negative, and the fast and slow axes are reversed.

4 Implications for Optics

Spatial-dispersion-induced birefringence and index anisotropy in CaF_2 are responsible for a number of effects that can severely degrade the performance of precision optics. These effects include wavefront aberrations, ray splitting,

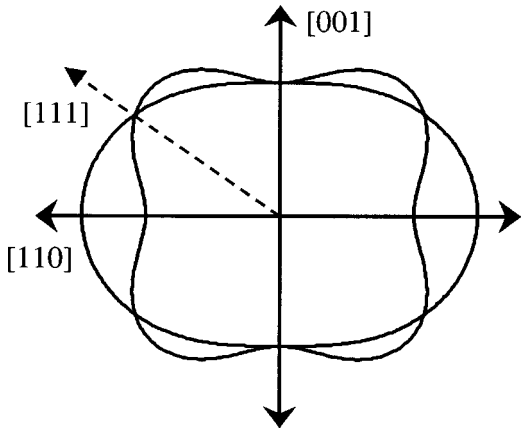

Fig. 10 Slice of the index surface of Fig. 9 in a $\{\bar{1}10\}$ plane. The surfaces touch in the nonbirefringent $\langle 001\rangle$ and $\langle 111\rangle$ directions. They are maximally split in the $\langle 110\rangle$ directions (cf. Fig. 6).

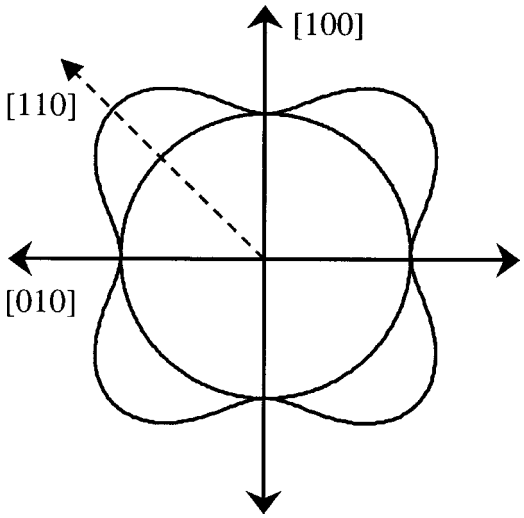

Fig. 11 Slice of the index surface of Fig. 9 in a {001} plane. The surfaces touch in the nonbirefringent ⟨100⟩ directions. They are maximally split in the ⟨011⟩ directions (cf. Figs. 7 and 8).

altered polarization states, and aberrations due to average index anisotropy. Since the magnitudes of these effects for CaF_2 near 157 nm are in general far larger than tolerances, they must be dealt with and designed around. For example, the intrinsic birefringence in CaF_2 at 157.6 nm, 11.2 nm/cm, is over ten times the industry target birefringence specification of 1 nm/cm for 157 nm lithography.[17]

In general, a light ray entering a birefringent crystal splits into two propagating eigenstates with orthogonal linear polarizations and different propagation directions $\hat{\mathbf{q}}$.

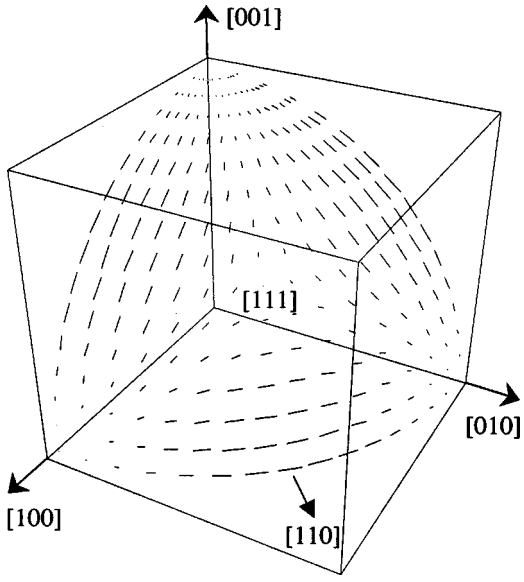

Fig. 12 Birefringence indicated for propagation directions in one octant of a sphere, by plot of large-index (slow axis) polarization eigenvectors. The magnitude of the polarization vector is scaled to the value of the index difference for each propagation direction. The figure shows birefringence zeros in the ⟨001⟩ and ⟨111⟩ directions and maxima in the ⟨110⟩ directions. The figure assumes $(n_{\langle 1\bar{1}0\rangle} - n_{\langle 001\rangle})$ is positive. For CaF_2 near 157 nm the value is negative, and the fast and slow axes are reversed.

Each of the two polarization states experiences a different index, and thus accumulates a different optical path length traveling through the crystal. For precision optical systems with many lenses, this gets rapidly complicated. For a sufficiently small birefringence, the ray splitting effects can be neglected, and the birefringence effect can be characterized merely by a relative phase shift between the polarization states. However, the measured birefringence in CaF_2 near 157 nm of 11.2 nm/cm may be on the margins where this approximation is valid. A relative shift in phase as large as $\sim\lambda/10$ causes wavefront aberrations that degrade imaging quality below the ideal diffraction limit. For anticipated photolithography step and scan systems with 20 or so lenses with randomly oriented crystal axes, and a total optical path length ~ 1 m, the wavefront aberrations can far exceed design specifications, and corrections are required. A related but distinct issue is that the average index also has an anisotropy far exceeding design tolerances. This must be corrected for as well.

4.1 *Lens Orientation*

For the special case of light rays traveling through a CaF_2 crystal in a ⟨001⟩ or ⟨111⟩ direction, the material exhibits no birefringence. Thus for lenses with axis of symmetry oriented in a ⟨001⟩ or ⟨111⟩ direction, paraxial rays suffer little effect. Further, as can be seen from Fig. 6, the average index has extrema in the ⟨001⟩ and ⟨111⟩ directions and is relatively insensitive to propagation direction near these axes. However, high resolution imaging requires large numerical apertures, involving a large cone of rays about the central axis. As can be seen from Fig. 6, for ⟨111⟩-oriented lenses, the birefringence reaches about 1/3 of its maximum value for propagation directions only about 10° off axis. The maximum effect is $\cos^{-1}[(2/3)^{1/2}] \approx 35°$ away. This rapid increase is a result of the large slope of the birefringence through zero, which is due to the threefold crystal symmetry in that direction. Near a ⟨001⟩ direction, the fourfold crystal symmetry requires there be an extremum (zero slope) in birefringence in this direction. This stationary nature of the effect near a ⟨001⟩ direction results in a much weaker birefringence increase for angles close to the axis. The maximum effect is 45° away. Thus ⟨001⟩-oriented lenses exhibit less birefringence than ⟨111⟩-oriented lenses for a given numerical aperture, up to cone angles including ⟨110⟩ directions. However, because of the high numerical apertures required for high-resolution imaging, substantial corrections are required even for ⟨001⟩-oriented lenses, in 157 nm lithography optics designs.

4.2 *Compensation by Crystal Axis Clocking*

While the intrinsic nature of the birefringence is its most disturbing quality since it cannot be reduced by material improvements in a pure material, it is also its redeeming quality. The predictability and high symmetry of the effect can be exploited for correction by combining lenses with different crystal axis orientations.[1–3,10–12]

The threefold symmetry of the effect about a ⟨111⟩ CaF_2 crystal axis, as seen by the eigenvector plot of Fig. 12, ensures that the phase retardation between different polarization states of light traveling symmetrically through a ⟨111⟩-oriented plate or lens will have a threefold symmetry.

Then the effect of a second ⟨111⟩-oriented plate or lens, with its transverse crystal axes rotated relatively by odd multiples of 60°, is to partially compensate for this azimuthal variation in the relative phase retardation. Similarly, the fourfold symmetric azimuthal variation in the relative phase retardation resulting from light traveling through a ⟨001⟩-oriented plate or lens can be partially compensated by including in the light path a second ⟨001⟩ plate or lens with its transverse crystal axes rotated by odd multiples of 45°. Both of these combinations still leave radial dependences to the relative phase retardations. However, by inspecting the eigenvector plot of Fig. 12, along with the angular dependence shown in Fig. 6, it can be seen that the radial dependences of the relative phase retardations for the ⟨111⟩ and ⟨001⟩ clocked pairs are of opposite sign. Thus combining these pairs can be used to reduce the radial dependence as well.[11,12]

Simulations show that for parallel plates with appropriate thicknesses, the relative phase retardations from the birefringence can be compensated nearly perfectly.[12] Commercial optical modeling software have been upgraded using the results of Sec. 3.4 to take account of the intrinsic birefringence effects in realistic optical design. Simulations have shown that, for realistic lens systems, the residual wavefront aberrations and their resulting imaging aberrations can be reduced by this method to acceptable levels for 157 nm lithography.[12]

Thus correction schemes based on crystal orientation clocking have been shown to be capable of adequately correcting for the aberrations caused by intrinsic birefringence in CaF_2. There is, however, a penalty for this. Besides the added design complexity entailed, the requirement for clocking to compensate for intrinsic birefringence effects reduces the degrees of freedom available for lens-element clocking to compensate for surface figure and index homogeneity aberrations. This may require even tighter tolerances for these parameters in 157 nm lithography systems.

5 Conclusions

We have described in detail the effect of the finite photon wave vector (spatial dispersion) on the refractive index properties in cubic crystals with the crystal structure of CaF_2. The theory predicts a breakdown of the isotropic optical properties at short wavelength, resulting in a birefringence and index inhomogeneity. We have fully characterized this behavior, and shown that it depends on only a single parameter for a given material at a given wavelength. The effect has interesting symmetries, and new approaches are required for precision optics in the UV with this heptaxial optical behavior. Our measurement of the single parameter for CaF_2 has shown that the magnitude of the effect for this material far exceeds the birefringence target specification for 157 nm lithography. Previous 157 nm lithography system designs ignoring this effect will not work. However, exploiting the high symmetry of the effect, compensation schemes based on combining optical elements with different crystal-axis orientations have been shown to adequately reduce the aberrations resulting from the effect. Still, for precision optics design in the VUV using CaF_2, it is now generally recognized that the crystal axis orientations for all CaF_2 refractive elements will have to be carefully controlled to minimize the intrinsic birefringence effects.

Acknowledgments

We gratefully acknowledge the support of the Office of Microelectronics Programs at NIST and International SEMATECH.

References

1. J. H. Burnett, Z. H. Levine, and E. L. Shirley, ''Intrinsic birefringence in 157 nm materials,'' in *2nd International Symposium on 157 nm Lithography*, R. Harbison, Ed., International SEMATECH, Austin, TX (2001).
2. J. H. Burnett, Z. H. Levine, and E. L. Shirley, ''Intrinsic birefringence in 157 nm materials,'' in *Calcium Fluoride Birefringence Workshop*, R. Harbison, Ed., International SEMATECH, Austin, TX (2001).
3. J. H. Burnett, Z. H. Levine, and E. L. Shirley, ''Intrinsic birefringence in calcium fluoride and barium fluoride,'' *Phys. Rev. B* **64**, 241102 (2001).
4. H. A. Lorentz, *Collected Papers II*, pp. 1–119, esp. p. 79, Martinus Nijohff, The Hague (1936); originally Verh. K. Akad. Wet. Amsterdam, Afd. Natuurkd. **18** (1878).
5. H. A. Lorentz, *Collected Papers III*, pp. 314–320, Martinus Nijohff, The Hague (1936); originally *Proc. Acad. Amsterdam* **24**, 333 (1921).
6. J. Pastrnak and K. Vedam, *Phys. Rev. B* **3**, 2567 (1971).
7. P. Y. Yu and M. Cardona, *Solid State Commun.* **9**, 1421 (1971).
8. http://physics.nist.gov/DUVBirefring
9. D. Krähmer, ''Intrinsic birefringence in CaF_2,'' in *Calcium Fluoride Birefringence Workshop*, R. Harbison, Ed., International SEMATECH, Austin, TX (2001).
10. K. Nattermann, ''Birefringence of CaF_2,'' in *Calcium Fluoride Birefringence Workshop*, R. Harbison, Ed., International SEMATECH, Austin, TX (2001).
11. N. Shiraishi, S. Owa, Y. Omura, T. Ozawa, and I. Tanaka, ''Current status of Nikon's investigation on CaF_2 intrinsic birefringence,'' in *Calcium Fluoride Birefringence Workshop*, R. Harbison, Ed., International SEMATECH, Austin, TX (2001).
12. N. Shiraishi, S. Owa, Y. Omura, T. Aoki, Y. Matsumoto, J. Nishikawa, and I. Tanaka, ''Progress of Nikon's F_2 exposure tool development,'' in *Optical Microlithography XV*, A. Yen, Ed., *Proc. SPIE,* **4691**, 594–601 (2002).
13. J. F. Nye, *Physical Properties of Crystals*, Oxford Science Publications, Oxford (1985).
14. V. M. Agranovich and V. L. Ginzburg, *Crystal Optics with Spatial Dispersion and Excitions*, 2nd ed., Springer, New York (1984).
15. H. J. Juretschke, *Crystal Physics*, Benjamin, London (1974).
16. L. D. Landau and E. M. Lifshitz, *Electrodynamics of Continuous Media*, pp. 313–321, Pergamon, Oxford (1960).
17. A. K. Bates, in *Proceedings of the First International Symposium on 157 nm Lithography*, R. Harbison, Ed., p. 377, International SEMATECH, Austin, TX (2000).